



Magnons and spinons in $\text{Ba}_2\text{CoTeO}_6$: A composite system of isolated spin- $\frac{1}{2}$ triangular Heisenberg-like and frustrated honeycomb Ising-like antiferromagnets

Yuki Kojima ^{1,*}, Nobuyuki Kurita,¹ Hidekazu Tanaka ^{1,†} and Kenji Nakajima^{2,3}

¹*Department of Physics, Tokyo Institute of Technology, Meguro, Tokyo 152-8551, Japan*

²*Materials and Life Science Division, J-PARC Center, Tokai, Ibaraki 319-1195, Japan*

³*Materials Sciences Research Center, Japan Atomic Energy Agency, Sayo, Hyogo 679-5148, Japan*



(Received 11 November 2021; revised 20 December 2021; accepted 11 January 2022; published 25 January 2022)

We report the neutron scattering results for magnetic orderings and excitations in $\text{Ba}_2\text{CoTeO}_6$ composed of two subsystems, A and B, which are described as an $S = 1/2$ triangular Heisenberg-like antiferromagnet and a frustrated honeycomb Ising-like antiferromagnet, respectively. We found that the excitation spectra of both subsystems are well separated and independent of each other. Stripy ordering of Ising-like subsystem B was confirmed below $T_{N1} = 12.0$ K, whereas the elastic scattering for subsystem A displays sharp streaks along $(1/3, 1/3, L)$ and $(2/3, 2/3, L)$ at 0.30 K ($\ll T_{N2} = 3.0$ K). These findings reveal that subsystems A and B are almost perfectly decoupled. The excitation spectrum of subsystem A is composed of two single-magnon branches with rotonlike minima at the M point and a clearly structured intense continuum, which is similarly observed in $\text{Ba}_3\text{CoSb}_2\text{O}_9$. Dispersion curves for subsystem B can be described by linear spin wave theory within the third-neighbor exchange interaction.

DOI: [10.1103/PhysRevB.105.L020408](https://doi.org/10.1103/PhysRevB.105.L020408)

The ground state of a two-dimensional (2D) spin- $\frac{1}{2}$ triangular-lattice Heisenberg antiferromagnet (TLHAF) with nearest-neighbor exchange interaction at zero magnetic field has been considered to be an ordered state with 120° structure [1–6] rather than a spin liquid state like the resonating-valence-bond (RVB) state [7]. However, the problem of whether the RVB state vanishes completely or survives in the ground state of the $S = 1/2$ TLHAF has not been resolved, although it seems that the ordered state and the RVB state are mutually exclusive. Studying the static magnetic properties appears to be insufficient to solve this problem; thus, a study of magnetic excitations is necessary. Note that the $S = 1/2$ TLHAF exhibits a wide magnetization plateau at one third of the saturation magnetization stabilized by quantum fluctuation [8–18].

In contrast to the ground state properties, the magnetic excitations in the $S = 1/2$ TLHAF are less well understood. The theoretical consensus appears to be limited for single-magnon excitations as follows: the excitation energy is significantly renormalized downward in a large area of the Brillouin zone, although the dispersion relation of low-energy excitations near the K point is described by linear spin wave theory (LSWT) [19–24]. In addition, the dispersion curve shows a rotonlike minimum at the M point, the origin of which has been interpreted to be spinon-antispinon pairs with each having spin $\frac{1}{2}$ [20]. However, theoretical consensus for the excitation continuum that reflects the characteristics of magnetic quasiparticles is also limited.

The predictions for the single-magnon excitations were partly confirmed by inelastic neutron scattering (INS) experiments on $\text{Ba}_3\text{CoSb}_2\text{O}_9$ [25–28], which approximates an $S = 1/2$ TLHAF [29–37]. However, the observed intense structured excitation continuum extending to high energies was markedly different from theory [24,27]. The features of an excitation spectrum, which cannot be described by LSWT, appeared to be strongly indicative of fractionalized excitations. The results of INS experiments on $\text{Ba}_3\text{CoSb}_2\text{O}_9$ motivated the theoretical studies of magnetic excitations based on spinon excitations [38–41]. In particular, approaches based on the RVB-like state with spinon excitations successfully reproduced the dispersion minima at both the M and Y points depicted in Fig. 1(d) [39,40]. These theoretical results demonstrated that the inherent quantum fluctuations still retain the characteristics of the RVB state even in the ordered ground state.

For the experimental establishment of a universal excitation spectrum for the $S = 1/2$ TLHAF, we need a model system with better two-dimensionality and smaller anisotropy than $\text{Ba}_3\text{CoSb}_2\text{O}_9$. $\text{Ba}_2\text{CoTeO}_6$, with a trigonal crystal structure [42], is a unique antiferromagnet composed of two highly frustrated subsystems, A and B, as shown in Fig. 1(a) [43]. Subsystem A is expressed as an $S = 1/2$ TLHAF with small XY-like exchange anisotropy. Subsystem B is composed of two uniform triangular lattices of Co_B^{2+} ions with effective spin $\frac{1}{2}$. Because these two triangular lattices are strongly coupled by exchange interactions J_1 and J_3 and Co_B^{2+} is affected by a strong trigonal crystal field due to the distortion of a Co_BO_6 octahedron, subsystem B is described as a frustrated honeycomb-lattice Ising-like antiferromagnet when projected onto the ab plane, as shown in Fig. 1(b). $\text{Ba}_2\text{CoTeO}_6$

*kojima.y.ai@m.titech.ac.jp

†tanaka@lee.phys.titech.ac.jp

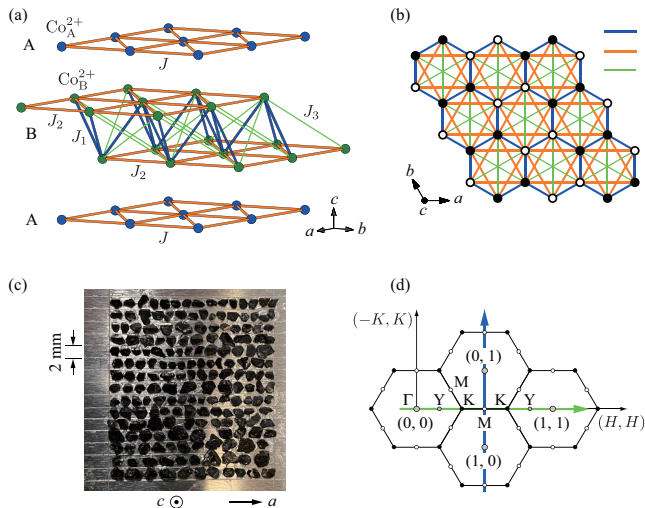


FIG. 1. (a) Magnetic subsystems A and B in $\text{Ba}_2\text{CoTeO}_6$. Thick blue and orange lines and thin green lines in subsystem B depict exchange interactions J_1 , J_2 , and J_3 , respectively. (b) Exchange network and stripy spin structure below T_{N1} in subsystem B viewed along the c axis. Solid and open circles denote up and down spins, respectively, reported in Ref. [42]. (c) Photograph of $\text{Ba}_2\text{CoTeO}_6$ single crystals coaligned on an aluminum plate for the present INS experiment. The wide plane is the crystallographic c plane. The a axis is parallel to the horizontal direction. (d) Two-dimensional reciprocal lattice for triangular layers in subsystems A and B.

undergoes successive magnetic phase transitions at $T_{N1} = 12.0$ and $T_{N2} = 3.0$ K, which correspond to the orderings of subsystems B and A, respectively [43]. Previous magnetic and thermodynamic measurements [43] and electron spin resonance (ESR) experiments [44] suggested that these two subsystems are almost decoupled. In this Letter, we demonstrate that the excitation spectra of these two subsystems are well separated and there is no correlation between their excitations, although the distance between neighboring Co_A^{2+} and Co_B^{2+} ions is close to that between neighboring two Co_A^{2+} ions. We show that an almost perfectly isolated layer of the $S = 1/2$ TLHAF is realized in $\text{Ba}_2\text{CoTeO}_6$ and that its excitation spectrum is universal in the $S = 1/2$ TLHAF. We also show that excitation spectrum for Ising-like subsystem B can be well described by the exchange model shown in Fig. 1(b) and determine its exchange parameters. Detailed knowledge of the exchange parameters of subsystem B is essential to understand the unusual multiple stepwise magnetization process caused by strong frustration on a honeycomb lattice [43].

Single crystals of $\text{Ba}_2\text{CoTeO}_6$ with a typical size of $2 \times 2 \times 0.3$ mm³ were grown by the same procedures as described in Ref. [43]. Single-crystal INS experiments were performed using the cold-neutron disk chopper spectrometer AMATERAS installed in the Materials and Life Science Experimental Facility (MLF) at the Japan Proton Accelerator Research Complex (J-PARC) [45]. Approximately 400 pieces of single crystals weighing about 1.3 g were coaligned on two aluminum plates along the $(1, 1, 0)$ and $(0, 0, 1)$ directions in the horizontal plane as shown in Fig. 1(c) using hydrogen-free CYTOP as the glue. The mosaic spread was about 3° . The sample was cooled to 0.30 K using a

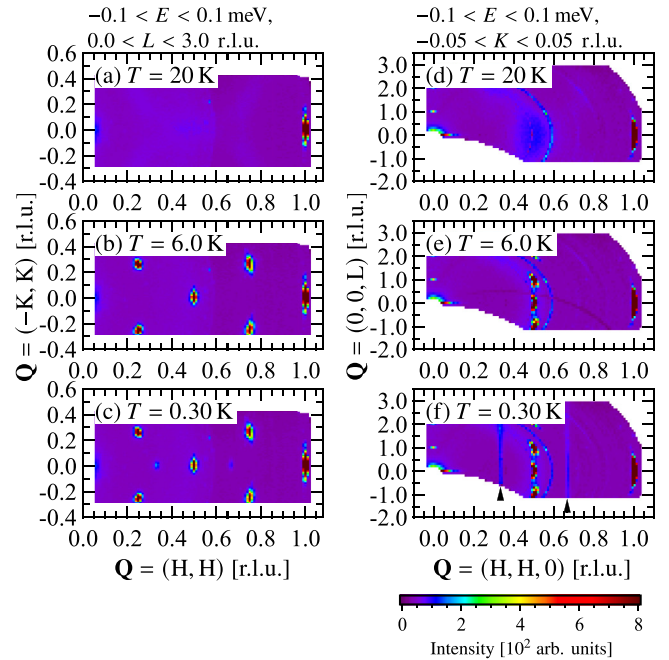


FIG. 2. (a)–(c) ENS intensity maps in the 2D reciprocal lattice measured with $E_i = 3.6$ meV at $T = 20$ K ($>T_{N1}$), 6.0 K ($T_{N1} > T > T_{N2}$), and 0.30 K ($\ll T_{N2}$), respectively. Averaged energy and momentum ranges are shown. (d)–(f) ENS intensity maps in the (H, H, L) plane, where the scattering intensity was averaged for $-0.05 \leq K \leq 0.05$ along $\mathbf{Q} = (-K, K, 0)$. Strong intensities around $\mathbf{Q} = (0, 0)$ due to the direct beam are masked in (a)–(f). Two triangles in (f) indicate diffuse streak patterns along $\mathbf{Q} = (1/3, 1/3, L)$ and $(2/3, 2/3, L)$. Curved streaks in (d)–(f) arise from a nonmagnetic origin.

^3He refrigerator. Scattering data were collected by rotating the sample around the vertical $(-1, 1, 0)$ direction by the multi- E_i technique with a set of incident neutron energies $E_i = 3.6, 5.6, 9.7,$ and 20.9 meV. Elastic energy resolutions are given by $\Delta E_i = 0.14, 0.3, 0.6,$ and 1.8 meV, respectively. All the data were analyzed using the software suite UT-SUSEMI [46]. Figures 2(a)–2(c) show the intensity maps of elastic neutron scattering (ENS) in the 2D reciprocal lattice plane measured with $E_i = 3.6$ meV at $T = 20$ K ($>T_{N1} = 12.0$ K), 6.0 K ($T_{N1} > T > T_{N2} = 3.0$ K), and 0.30 K ($\ll T_{N2}$), respectively, where the scattering intensity was averaged in a momentum range of $0 \leq L \leq 3$. Figures 2(d)–2(f) show the ENS intensity maps in the (H, H, L) plane measured at $T = 20, 6.0,$ and 0.30 K, respectively. The strong Bragg peak commonly observed at $\mathbf{Q} = (1, 1, 0)$ is a nuclear peak. As the temperature decreases below $T_{N1} = 12.0$ K, magnetic Bragg peaks emerge at $\mathbf{Q} = (1/2, 0, 0)$ and equivalent positions, which is consistent with the results of a previous study by Ivanov *et al.* [42]. These magnetic Bragg peaks are attributed to a stripy order of Ising-like subsystem B, as shown in Fig. 1(b), characterized by the propagation vector $\mathbf{k} = (1/2, 0, 0)$.

With a further decrease in temperature to $T = 0.30$ K, which is much lower than $T_{N2} = 3.0$ K, sharp streak patterns are observed along $\mathbf{Q} = (1/3, 1/3, L)$ and $(2/3, 2/3, L)$, as shown in Fig. 2(f). After averaging the scattering intensity

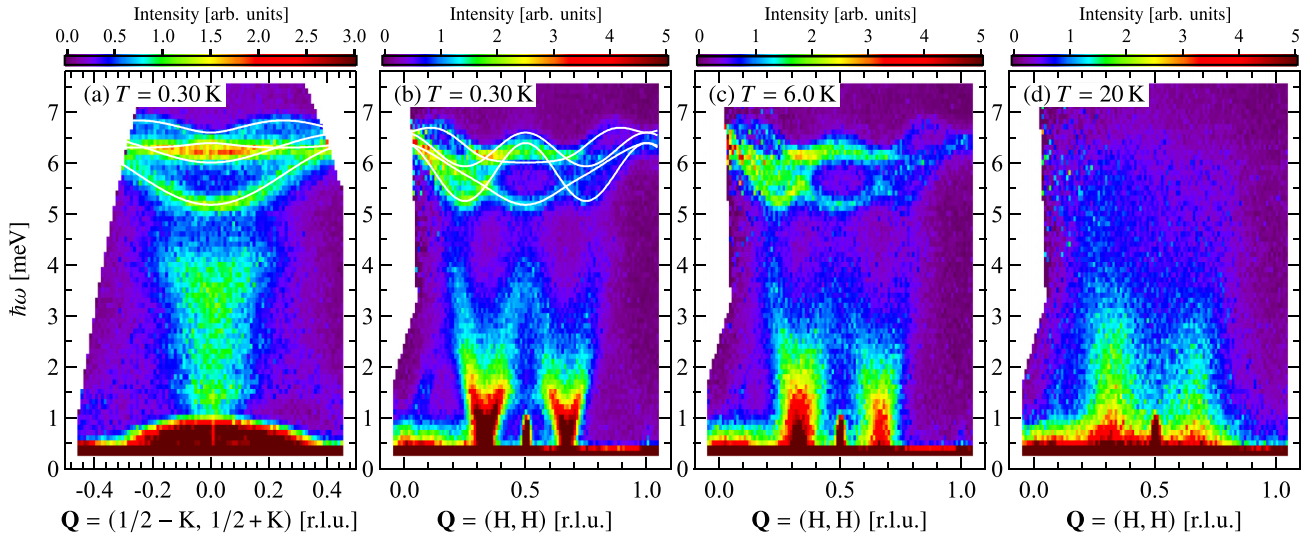


FIG. 3. (a) and (b) Excitation spectra of Ba₂CoTeO₆ measured with $E_i = 9.7$ meV at $T = 0.30$ K along high-symmetry directions $\mathbf{Q} = (1/2 - K, 1/2 + K)$ and (H, H) , shown by blue and green arrows in Fig. 1(d), respectively. (c) and (d) Thermal evolution of excitation spectrum along $\mathbf{Q} = (H, H)$ measured at $T = 6.0$ and 20 K, respectively. The scattering intensities were averaged in a range of $-3 \leq L \leq 3$ to map the scattering intensity in the 2D reciprocal lattice assuming good two-dimensionality. A broad inelastic signal along $\mathbf{Q} = (1/2 - K, 1/2 + K)$ below 1 meV in (a), which corresponds to pointed signals at $(1/2, 1/2)$ in (b)–(d), is attributable to spurious scattering from the sample environment. The solid lines in (a) and (b) are dispersion curves of Ising-like subsystem B calculated on the basis of LSWT using the J_1 - J_2 - J_3 XXZ model of Eq. (2) with the exchange parameters shown in the text.

over L , these streaks are observed as sharp spots in the 2D reciprocal lattice, as shown in Fig. 2(c). This result indicates that below T_{N2} , the 120° structure is constructed in a triangular layer of subsystem A, whereas the interlayer ordering is not long range but short range. This is an unexpected result because specific heat displays a sharp cusp anomaly at T_{N2} , suggestive of the three-dimensional ordering [43].

Figures 3(a) and 3(b) show the excitation spectra of Ba₂CoTeO₆ in high-symmetry directions $\mathbf{Q} = (1/2 - K, 1/2 + K)$ and (H, H) , respectively, measured with $E_i = 9.7$ meV at $T = 0.30$ K. The scattering intensities were averaged in the range of $-3 \leq L \leq 3$ to map the scattering intensity in the 2D reciprocal lattice. We confirmed good two-dimensionality from the observation that the excitation spectrum is dispersionless along the c^* direction, as shown in Fig. 4(b). The structured excitation spectrum at $T = 0.30$ K becomes very indistinct at $T = 20$ K, as shown in Fig. 3(d). The scattering intensity at around 6 meV decreases rapidly at $T = 20$ K. This result verifies that the origins of the excitation spectra shown in Fig. 3 are magnetic.

The excitation spectrum at $T = 0.30$ K can be divided into two parts, low-energy excitation ($\hbar\omega < 5$ meV) and high-energy excitation ($5 < \hbar\omega < 7$ meV). In previous studies [43,44], the predominant exchange interactions were estimated as $J \simeq 1.8$ meV for subsystem A and $J_1 \simeq 4.8$ and $J_2 \simeq 2.4$ meV for subsystem B, where the exchange constants were estimated on the basis of the J_1 - J_2 honeycomb-lattice Ising antiferromagnet without XY components. Thus, we can deduce that the low- and high-energy spectra originate in subsystems A and B, respectively. This can also be confirmed from the temperature evolution of the excitation spectrum shown in Figs. 3(c) and 3(d). At $T = 6.0$ K, which is twofold T_{N2} , the low-energy spectrum becomes indistinct, whereas

the high-energy spectrum remains unchanged. These results show that the low- and high-energy spectra have different sources, which exhibit magnetic orderings separately at T_{N2} and T_{N1} , respectively. In a previous magnetization study of Ba₂CoTeO₆, successive transitions with a sharp stepwise magnetization curve characteristic of the ordered state in

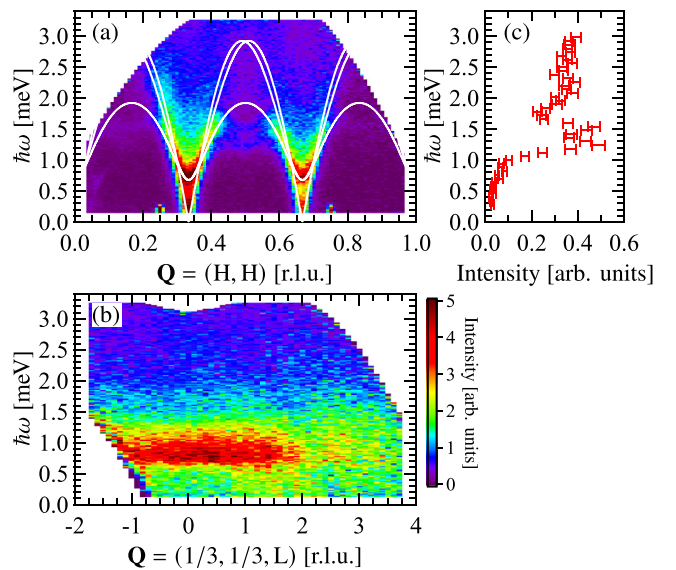


FIG. 4. Energy-momentum map of low-energy excitations of Ba₂CoTeO₆ measured with $E_i = 3.6$ meV at $T = 0.30$ K along (a) $\mathbf{Q} = (H, H)$, where the scattering intensities were averaged over L , and (b) $\mathbf{Q} = (1/3, 1/3, L)$. The solid lines in (a) are LSWT dispersion curves calculated with $J = 1.85$ meV and $\Delta = 0.040$. (c) Scattering intensity at $\mathbf{Q} = (1/2, 1/2)$ as a function of energy.

an Ising-like antiferromagnet were observed at $T = 4.2$ K ($T_{N2} < T < T_{N1}$) for magnetic fields parallel to the c axis [43]. The result of the magnetization measurements confirms that T_{N1} corresponds to the ordering temperature of Ising-like subsystem B. From the energy scales and temperature evolution of the excitation spectrum, the sources of the low- and high-energy spectra can be subsystems A and B, respectively. Note that the excitation spectra of subsystem B show no change through T_{N2} . Given that subsystems A and B are exchange coupled, the change in the dispersion curves of subsystem B will be observed above and below T_{N2} . Thus, we can confirm that subsystems A and B are almost perfectly decoupled.

Figure 4(a) shows the spectrum of low-energy excitations from subsystem A along $\mathbf{Q} = (H, H)$ measured at $T = 0.30$ K with $E_i = 3.6$ meV, where the scattering intensities were averaged in the range of $0 \leq L \leq 3$ assuming good two-dimensionality. Figure 4(b) shows the spectrum of low-energy excitations from subsystem A along $\mathbf{Q} = (1/3, 1/3, L)$ measured at $T = 0.30$ K with $E_i = 3.6$ meV. It is notable that the excitations are completely dispersionless along $\mathbf{Q} = (1/3, 1/3, L)$ compared with those from $\text{Ba}_3\text{CoSb}_2\text{O}_9$, in which low-energy single-magnon excitations are dispersive along $\mathbf{Q} = (1/3, 1/3, L)$ owing to the finite interlayer interactions [26]. This result, together with the ENS result shown in Fig. 2(f), demonstrates that each triangular layer of subsystem A is almost perfectly isolated. It can be understood that Ising-like subsystem B undergoes magnetic ordering at $T_{N1} = 12.0$ K without the help of the interlayer exchange interaction because the strong easy-axis exchange anisotropy can stabilize the magnetic ordering. However, the magnetic ordering at $T_{N2} = 3.0$ K for subsystem A with the small easy-plane anisotropy has not yet been fully explained because 2D Heisenberg and XY-like antiferromagnets exhibit no long-range order at finite temperature [47,48].

Here we compare single-magnon excitations in subsystem A with LSWT. We consider the 2D Heisenberg model with a weak XY anisotropy expressed as

$$\mathcal{H}_A = J \sum_{\langle i, j \rangle} (\mathbf{S}_i \cdot \mathbf{S}_j - \Delta S_i^z S_j^z), \quad (1)$$

where J and Δ (>0) are the coupling constant and the anisotropy parameter, respectively. The LSWT dispersion curves with $J = 1.85$ meV and $\Delta = 0.040$ describe well the experimental dispersion curves below 1 meV in the vicinity of the K point at $\mathbf{Q} = (1/3, 1/3)$ and $(2/3, 2/3)$, as shown Fig. 4(a). These exchange parameters also coincide with those estimated from the saturation field of subsystem A and the zero-field gap obtained by ESR measurements [43,44]. The farther the wave vector moves away from the K point, the more rapidly the excitation energy deviates downward from the LSWT dispersion, as predicted by theory [19–24,38–40] and as observed in $\text{Ba}_3\text{CoSb}_2\text{O}_9$ [26,28]. It is notable that two single-magnon dispersion curves display rotonlike minima at $\mathbf{Q} = (1/2, 1/2)$. Figure 4(c) shows scattering intensity at $\mathbf{Q} = (1/2, 1/2)$ as a function of energy. The dispersion minima with energies of $\hbar\omega = 1.25$ and 1.55 meV correspond to the minima at the M and Y points in the single branch, respectively.

Overall, the features of the excitation spectrum of subsystem A are very similar to those observed in $\text{Ba}_3\text{CoSb}_2\text{O}_9$ [26,28]. Downward renormalized single-magnon excitation energies, two rotonlike minima of the dispersion curves at $\mathbf{Q} = (1/2, 1/2)$, and an intense structured excitation continuum extending to at least 5 meV, which is approximately three times larger than that in the exchange interaction J shown in Figs. 3(a) and 3(b), are the common observations. From these observations, we conclude that the low-energy part of the excitation spectrum of $\text{Ba}_2\text{CoTeO}_6$ and the excitation spectrum of $\text{Ba}_3\text{CoSb}_2\text{O}_9$ are universal in the $S = 1/2$ TLHAFs. The difference between $\text{Ba}_2\text{CoTeO}_6$ and $\text{Ba}_3\text{CoSb}_2\text{O}_9$ is that the intensities of single-magnon excitations around $\mathbf{Q} = (1/2, 1/2)$ in $\text{Ba}_2\text{CoTeO}_6$ are considerably weaker than those around the K point. We speculate that the spectral difference between these two systems arises from the difference in their interlayer interactions.

Recent theories based on the RVB-like state with spinon excitations successfully reproduced two rotonlike minima of the dispersion curves at $\mathbf{Q} = (1/2, 1/2)$ [39,40]. The RVB-based approaches also roughly describe the features of the excitation continuum observed in $\text{Ba}_2\text{CoTeO}_6$ and $\text{Ba}_3\text{CoSb}_2\text{O}_9$. For these reasons, we deduce that the inherent quantum fluctuations still have the characteristics of the RVB state even in the ordered ground state of the $S = 1/2$ TLHAFs.

Next, we analyze the dispersion curves of the high-energy single-magnon excitations in an energy range of $5 < \hbar\omega < 7$ meV, which originate in subsystem B. Because the observed spectrum is dispersive, which indicates the finite XY component, we consider the following XXZ model on a honeycomb lattice with up to the third-neighbor J_1 , J_2 , and J_3 exchange interactions, as shown in Fig. 1(b):

$$\mathcal{H}_B = \sum_{v=1}^3 \sum_{\langle i, j \rangle_v} J_v [S_i^z S_j^z + \delta (S_i^x S_j^x + S_i^y S_j^y)], \quad (2)$$

where $\langle i, j \rangle_v$ is the v th nearest-neighbor coupling pairs. The z axis is taken to be along the crystallographic c axis. The anisotropy parameter δ is assumed to be the same for all interactions because the exchange anisotropy is generally determined by the distortion of a single CoO_6 octahedron.

In the previous magnetization measurements in $\text{Ba}_2\text{CoTeO}_6$ [43], magnetization plateaus at one third and one half of the saturation magnetization were observed for magnetic fields parallel to the c axis. Critical fields H_{c1} and H_{c2} for transitions to the 1/3- and 1/2-magnetization plateau states and the saturation field H_s were found to be $H_{c1} = 12.3$, $H_{c2} = 14.8$, and $H_s = 39.0$ T. These transition fields were analyzed within the context of a J_1 - J_2 Ising model. Here, we consider the third-neighbor ferromagnetic exchange interaction J_3 because the dispersion curves of subsystem B cannot be reproduced within the J_1 - J_2 model. Within the Ising model, the critical fields and saturation field are expressed as $H_{c1} = J_1 - 2J_3$, $H_{c2} = -(1/2)J_1 + 3J_2 + 4J_3$, and $H_s = (3/2)J_1 + 3J_2$, where $g_B^{\parallel} \mu_B$ is set to be unity for simplicity. The ferromagnetic J_3 interaction stabilizes the stripy order at zero magnetic field, which enhances the energy gap and destabilizes the 1/3-magnetization plateau state to reduce its field range. We calculate the

dispersion curves of subsystem B on the basis of LSWT under the constraint $H_{c1}/H_{c2} = 12.3/14.8$, which leads to $J_3 = 0.266J_1 - 0.468J_2$. We assume three types of magnetic domain with the stripy order. Solid lines in Figs. 3(a) and 3(b) are dispersion curves calculated with $J_1 = 2.94$, $J_2 = 2.37$, $J_3 = -0.328$ meV, and $\delta = 0.15$ and are in good agreement with experimental results. Although there are generally six excitation branches owing to three magnetic domains, only four branches are observed along two high-symmetry directions, $\mathbf{Q} = (1/2 - K, 1/2 + K)$ and (H, H) , shown by blue and green arrows in Fig. 1(d), respectively, because two domains are equivalent.

To conclude, we have presented excitation spectra of Ba₂CoTeO₆ composed of two subsystems, A and B, which are described as an $S = 1/2$ TLHAF with small XY-like exchange anisotropy and a frustrated honeycomb-lattice Ising-like antiferromagnet, respectively. We found that the magnetic ordering of subsystem A below T_{N2} has a 2D nature without long-range order along the c direction. We also found that excitation spectra from both subsystems are well separated

and independent of each other. These findings reveal that these two subsystems are almost perfectly decoupled and that an almost perfectly isolated layer of the $S = 1/2$ TLHAF is realized in subsystem A. We found that the excitation spectrum of subsystem A is almost the same as that of Ba₃CoSb₂O₉ when scaled by the exchange constant J , which shows that the excitation spectra of subsystem A and Ba₃CoSb₂O₉ are universal in $S = 1/2$ TLHAFs. We demonstrated on the basis of LSWT that dispersion curves of Ising-like subsystem B are well described by a J_1 - J_2 - J_3 XXZ model on a honeycomb lattice and determined its exchange parameters.

We express our sincere thanks to instrumental scientists S. Ohira-Kawamura and M. Kofu, and sample environment team members at the J-PARC MLF R. Takahashi and Y. Yamauchi for their technical support. This work was supported by Grants-in-Aid for Scientific Research from the Japan Society for the Promotion of Science (JP), 17H01142, 19K03711, and 20J22215. The experiments on AMATERAS were performed with the approval of J-PARC (Proposal No. 2019B0092).

-
- [1] D. A. Huse and V. Elser, Simple Variational Wave Functions for Two-Dimensional Heisenberg Spin-1/2 Antiferromagnets, *Phys. Rev. Lett.* **60**, 2531 (1988).
- [2] T. Jolicoeur and J. C. Le Guillou, Spin-wave results for the triangular Heisenberg antiferromagnet, *Phys. Rev. B* **40**, 2727 (1989).
- [3] B. Bernu, P. Lecheminant, C. Lhuillier, and L. Pierre, Exact spectra, spin susceptibilities, and order parameter of the quantum Heisenberg antiferromagnet on the triangular lattice, *Phys. Rev. B* **50**, 10048 (1994).
- [4] R. R. P. Singh and D. A. Huse, Three-Sublattice Order in Triangular- and Kagomé-Lattice Spin-Half Antiferromagnets, *Phys. Rev. Lett.* **68**, 1766 (1992).
- [5] S. R. White and A. L. Chernyshev, Néel Order in Square and Triangular Lattice Heisenberg Models, *Phys. Rev. Lett.* **99**, 127004 (2007).
- [6] O. Götze, J. Richter, R. Zinke, and D. Farnell, Ground-state properties of the triangular-lattice Heisenberg antiferromagnet with arbitrary spin quantum number s , *J. Magn. Magn. Mater.* **397**, 333 (2016).
- [7] P. Anderson, Resonating valence bonds: A new kind of insulator? *Mater. Res. Bull.* **8**, 153 (1973).
- [8] A. V. Chubukov and D. I. Golosov, Quantum theory of an antiferromagnet on a triangular lattice in a magnetic field, *J. Phys.: Condens. Matter* **3**, 69 (1991).
- [9] T. Nikuni and H. Shiba, Quantum fluctuations and magnetic structures of CsCuCl₃ in high magnetic field, *J. Phys. Soc. Jpn.* **62**, 3268 (1993).
- [10] A. Honecker, A comparative study of the magnetization process of two-dimensional antiferromagnets, *J. Phys.: Condens. Matter* **11**, 4697 (1999).
- [11] J. Alicea, A. V. Chubukov, and O. A. Starykh, Quantum Stabilization of the 1/3-Magnetization Plateau in Cs₂CuBr₄, *Phys. Rev. Lett.* **102**, 137201 (2009).
- [12] D. J. J. Farnell, R. Zinke, J. Schulenburg, and J. Richter, High-order coupled cluster method study of frustrated and unfrustrated quantum magnets in external magnetic fields, *J. Phys.: Condens. Matter* **21**, 406002 (2009).
- [13] T. Sakai and H. Nakano, Critical magnetization behavior of the triangular- and kagome-lattice quantum antiferromagnets, *Phys. Rev. B* **83**, 100405(R) (2011).
- [14] C. Hotta, S. Nishimoto, and N. Shibata, Grand canonical finite size numerical approaches in one and two dimensions: Real space energy renormalization and edge state generation, *Phys. Rev. B* **87**, 115128 (2013).
- [15] D. Yamamoto, G. Marmorini, and I. Danshita, Quantum Phase Diagram of the Triangular-Lattice XXZ Model in a Magnetic Field, *Phys. Rev. Lett.* **112**, 127203 (2014).
- [16] O. A. Starykh, Unusual ordered phases of highly frustrated magnets: A review, *Rep. Prog. Phys.* **78**, 052502 (2015).
- [17] D. Sellmann, X.-F. Zhang, and S. Eggert, Phase diagram of the antiferromagnetic XXZ model on the triangular lattice, *Phys. Rev. B* **91**, 081104(R) (2015).
- [18] T. Coletta, T. A. Tóth, K. Penc, and F. Mila, Semiclassical theory of the magnetization process of the triangular lattice Heisenberg model, *Phys. Rev. B* **94**, 075136 (2016).
- [19] O. A. Starykh, A. V. Chubukov, and A. G. Abanov, Flat spin-wave dispersion in a triangular antiferromagnet, *Phys. Rev. B* **74**, 180403(R) (2006).
- [20] W. Zheng, J. O. Fjærestad, R. R. P. Singh, R. H. McKenzie, and R. Coldea, Excitation spectra of the spin- $\frac{1}{2}$ triangular-lattice Heisenberg antiferromagnet, *Phys. Rev. B* **74**, 224420 (2006).
- [21] A. L. Chernyshev and M. E. Zhitomirsky, Spin waves in a triangular lattice antiferromagnet: Decays, spectrum renormalization, and singularities, *Phys. Rev. B* **79**, 144416 (2009).
- [22] A. Mezio, C. N. Sposetti, L. O. Manuel, and A. E. Trumper, A test of the bosonic spinon theory for the triangular antiferromagnet spectrum, *Europhys. Lett.* **94**, 47001 (2011).
- [23] M. Mourigal, W. T. Fuhrman, A. L. Chernyshev, and M. E. Zhitomirsky, Dynamical structure factor of the triangular-lattice antiferromagnet, *Phys. Rev. B* **88**, 094407 (2013).

- [24] E. A. Ghioldi, A. Mezio, L. O. Manuel, R. R. P. Singh, J. Oitmaa, and A. E. Trumper, Magnons and excitation continuum in XXZ triangular antiferromagnetic model: Application to $\text{Ba}_3\text{CoSb}_2\text{O}_9$, *Phys. Rev. B* **91**, 134423 (2015).
- [25] J. Ma, Y. Kamiya, T. Hong, H. B. Cao, G. Ehlers, W. Tian, C. D. Batista, Z. L. Dun, H. D. Zhou, and M. Matsuda, Static and Dynamical Properties of the Spin-1/2 Equilateral Triangular-Lattice Antiferromagnet $\text{Ba}_3\text{CoSb}_2\text{O}_9$, *Phys. Rev. Lett.* **116**, 087201 (2016).
- [26] S. Ito, N. Kurita, H. Tanaka, S. Ohira-Kawamura, K. Nakajima, S. Itoh, K. Kuwahara, and K. Kakurai, Structure of the magnetic excitations in the spin-1/2 triangular-lattice Heisenberg antiferromagnet $\text{Ba}_3\text{CoSb}_2\text{O}_9$, *Nat. Commun.* **8**, 235 (2017).
- [27] Y. Kamiya, L. Ge, T. Hong, Y. Qiu, D. L. Quintero-Castro, Z. Lu, H. B. Cao, M. Matsuda, E. S. Choi, C. D. Batista, M. Mourigal, H. D. Zhou, and J. Ma, The nature of spin excitations in the one-third magnetization plateau phase of $\text{Ba}_3\text{CoSb}_2\text{O}_9$, *Nat. Commun.* **9**, 2666 (2018).
- [28] D. Macdougall, S. Williams, D. Prabhakaran, R. I. Bewley, D. J. Voneshen, and R. Coldea, Avoided quasiparticle decay and enhanced excitation continuum in the spin- $\frac{1}{2}$ near-Heisenberg triangular antiferromagnet $\text{Ba}_3\text{CoSb}_2\text{O}_9$, *Phys. Rev. B* **102**, 064421 (2020).
- [29] Y. Shirata, H. Tanaka, A. Matsuo, and K. Kindo, Experimental Realization of a Spin-1/2 Triangular-Lattice Heisenberg Antiferromagnet, *Phys. Rev. Lett.* **108**, 057205 (2012).
- [30] H. D. Zhou, C. Xu, A. M. Hallas, H. J. Silverstein, C. R. Wiebe, I. Umegaki, J. Q. Yan, T. P. Murphy, J.-H. Park, Y. Qiu, J. R. D. Copley, J. S. Gardner, and Y. Takano, Successive Phase Transitions and Extended Spin-Excitation Continuum in the $S=\frac{1}{2}$ Triangular-Lattice Antiferromagnet $\text{Ba}_3\text{CoSb}_2\text{O}_9$, *Phys. Rev. Lett.* **109**, 267206 (2012).
- [31] T. Susuki, N. Kurita, T. Tanaka, H. Nojiri, A. Matsuo, K. Kindo, and H. Tanaka, Magnetization Process and Collective Excitations in the $S=1/2$ Triangular-Lattice Heisenberg Antiferromagnet $\text{Ba}_3\text{CoSb}_2\text{O}_9$, *Phys. Rev. Lett.* **110**, 267201 (2013).
- [32] G. Quirion, M. Lapointe-Major, M. Poirier, J. A. Quilliam, Z. L. Dun, and H. D. Zhou, Magnetic phase diagram of $\text{Ba}_3\text{CoSb}_2\text{O}_9$ as determined by ultrasound velocity measurements, *Phys. Rev. B* **92**, 014414 (2015).
- [33] G. Koutroulakis, T. Zhou, Y. Kamiya, J. D. Thompson, H. D. Zhou, C. D. Batista, and S. E. Brown, Quantum phase diagram of the $S = \frac{1}{2}$ triangular-lattice antiferromagnet $\text{Ba}_3\text{CoSb}_2\text{O}_9$, *Phys. Rev. B* **91**, 024410 (2015).
- [34] D. Yamamoto, G. Marmorini, and I. Danshita, Microscopic Model Calculations for the Magnetization Process of Layered Triangular-Lattice Quantum Antiferromagnets, *Phys. Rev. Lett.* **114**, 027201 (2015).
- [35] M. Li, A. Zelenskiy, J. A. Quilliam, Z. L. Dun, H. D. Zhou, M. L. Plumer, and G. Quirion, Magnetoelastic coupling and the magnetization plateau in $\text{Ba}_3\text{CoSb}_2\text{O}_9$, *Phys. Rev. B* **99**, 094408 (2019).
- [36] X. Z. Liu, O. Prokhnenko, D. Yamamoto, M. Bartkowiak, N. Kurita, and H. Tanaka, Microscopic evidence of a quantum magnetization process in the $S = \frac{1}{2}$ triangular-lattice Heisenberg-like antiferromagnet $\text{Ba}_3\text{CoSb}_2\text{O}_9$, *Phys. Rev. B* **100**, 094436 (2019).
- [37] N. A. Fortune, Q. Huang, T. Hong, J. Ma, E. S. Choi, S. T. Hannahs, Z. Y. Zhao, X. F. Sun, Y. Takano, and H. D. Zhou, Evolution of magnetic field induced ordering in the layered quantum Heisenberg triangular-lattice antiferromagnet $\text{Ba}_3\text{CoSb}_2\text{O}_9$, *Phys. Rev. B* **103**, 184425 (2021).
- [38] E. A. Ghioldi, M. G. Gonzalez, S.-S. Zhang, Y. Kamiya, L. O. Manuel, A. E. Trumper, and C. D. Batista, Dynamical structure factor of the triangular antiferromagnet: Schwinger boson theory beyond mean field, *Phys. Rev. B* **98**, 184403 (2018).
- [39] C. Zhang and T. Li, Resonating valence bond theory of anomalous spin dynamics of spin- $\frac{1}{2}$ triangular lattice Heisenberg antiferromagnet and its application to $\text{Ba}_3\text{CoSb}_2\text{O}_9$, *Phys. Rev. B* **102**, 075108 (2020).
- [40] F. Ferrari and F. Becca, Dynamical Structure Factor of the $J_1 - J_2$ Heisenberg Model on the Triangular Lattice: Magnons, Spinons, and Gauge Fields, *Phys. Rev. X* **9**, 031026 (2019).
- [41] R. Verresen, R. Moessner, and F. Pollmann, Avoided quasiparticle decay from strong quantum interactions, *Nat. Phys.* **15**, 750 (2019).
- [42] S. A. Ivanov, P. Nordblad, R. Mathieu, R. Tellgren, and C. Ritter, Neutron diffraction studies and the magnetism of an ordered perovskite: $\text{Ba}_2\text{CoTeO}_6$, *Dalton Trans.* **39**, 5490 (2010).
- [43] P. Chanlert, N. Kurita, H. Tanaka, D. Goto, A. Matsuo, and K. Kindo, Field-driven successive phase transitions in the quasi-two-dimensional frustrated antiferromagnet $\text{Ba}_2\text{CoTeO}_6$ and highly degenerate classical ground states, *Phys. Rev. B* **93**, 094420 (2016).
- [44] P. Chanlert, N. Kurita, H. Tanaka, M. Kimata, and H. Nojiri, Collective and local excitations in $\text{Ba}_2\text{CoTeO}_6$: A composite system of a spin- $\frac{1}{2}$ triangular-lattice Heisenberg antiferromagnet and a honeycomb-lattice $J_1 - J_2$ Ising antiferromagnet, *Phys. Rev. B* **96**, 064419 (2017).
- [45] K. Nakajima *et al.*, AMATERAS: A cold-neutron disk chopper spectrometer, *J. Phys. Soc. Jpn.* **80**, SB028 (2011).
- [46] Y. Inamura, T. Nakatani, J. Suzuki, and T. Otomo, Development status of software “Utsusemi” for chopper spectrometers at MLF, J-PARC, *J. Phys. Soc. Jpn.* **82**, SA031 (2013).
- [47] N. D. Mermin and H. Wagner, Absence of Ferromagnetism or Antiferromagnetism in One- or Two-Dimensional Isotropic Heisenberg Models, *Phys. Rev. Lett.* **17**, 1133 (1966).
- [48] P. C. Hohenberg, Existence of long-range order in one and two dimensions, *Phys. Rev.* **158**, 383 (1967).